JASA ARTICLE

Study of "half-integer" harmonics in recorder tones and some speculations about their origin

Nicholas Giordano[a] and Katherine L. Saenger[b]
Department of Physics, Auburn University, Auburn, Alabama 36832, USA

ABSTRACT:
The musical notes produced by recorders and other flue instruments consist primarily of spectral components with frequencies given approximately by nf_1, where n is an integer and f_1 is the fundamental frequency. However, the real tones of these instruments contain other spectral components that have been observed and discussed by a number of authors. We report a study of spectral components in the tones produced by recorders that are odd half-integer multiples of f_1, i.e., spectral components with frequencies $\left(n \pm \frac{1}{2}\right)f_1$. Our results, obtained through a combination of experimental and simulation studies of soprano recorders, suggest that these components are associated with the air flow in the vicinity of the window region and the labium edge. We also show that these half-harmonics can be suppressed by modifications of the instrument that alter the pattern of air flow in those regions. Speculations concerning the importance of the half-harmonics and the degree to which they are perceptible by a listener are briefly discussed.
© *2023 Acoustical Society of America*. https://doi.org/10.1121/10.0022327

(Received 8 May 2023; revised 11 October 2023; accepted 17 October 2023; published online 8 November 2023)

[Editor: Vasileios Chatziioannou] Pages: 2917–2927

I. INTRODUCTION AND BACKGROUND

Most of our understanding of the tones produced by recorders and other flue instruments starts with the geometry sketched in Fig. 1. An air jet emerges from a channel and impinges on a sharp edge called a labium. The interaction of this jet with the labium causes the jet to oscillate between trajectories that take it above and below the labium. This oscillating flow excites standing acoustic waves in the resonator, with the dominant standing wave frequency determined (in large part) by one of the resonant frequencies of the resonator. The feedback to the air jet causes its oscillation to synchronize with the standing wave frequency, with sound emitted strongly from both the open end of the resonator and the window region. The emitted sound contains large components at frequencies nf_1, where f_1 is the fundamental frequency and n is an integer. The strength of each frequency component in the spectrum depends on both its intrinsic strength at the source (determined by channel/labium geometry, etc.) and the degree to which that frequency gets amplified by the resonator.

This simple picture of sound production provides a useful qualitative explanation of the spectrum of a recorder tone. However, a careful examination of the spectra of real recorder tones reveals additional spectral components that can make clearly audible contributions to the tones of real instruments. There have been many studies of the spectra of real recorders (and the closely related tones of flue organ pipes), and theoretical work has successfully explained many of the observed deviations from an "ideal" harmonic spectrum.[1,2] However, there remain interesting spectral features that are not yet explained or understood.

One of these features can be described as "half-harmonics," i.e., spectral components with frequencies $\left(n \pm \frac{1}{2}\right)f_1$, where n is an integer (we will also refer to them as half-integer harmonics). A half-harmonic component with frequency $f_1/2$ corresponds to an oscillation with a period twice that of the fundamental spectral component, suggesting a possible connection with the period doubling route to chaos found in a variety of nonlinear dynamical systems (see, for example, Refs. 3 and 4). Several authors[5–8] have discussed the connection to this phenomenon in the context of different musical instruments, and noted that most of those cases involve an instrument with a noticeably anharmonic structural component, such as the player's lips in the case of a trombone, or reeds in cases such as a clarinet or bassoon. For the case of a recorder or flue instrument, we have found a number of results in the literature in which half-harmonics have (possibly or with some certainty) been observed experimentally,[9–14] although their presence was not remarked on by those authors. As far as we know, there is no quantitative or even qualitative theoretical treatment of period doubling in such instruments.

One goal of this paper is to describe new results for the half-harmonic tones that appear in the steady state spectrum of a soprano recorder at certain well-defined ranges of blowing pressure. While ours are not the first observations of these spectral features, a combination of experiments and simulations has enabled us to show that the process responsible for the half-harmonics takes place in the window/labium region (Fig. 1). We also demonstrate that simple modifications of the trajectory of the air jet as it emerges

[a]Email: njg0003@auburn.edu
[b]Also at: 115 Underhill Road, Ossining, NY 10562-4408, USA.

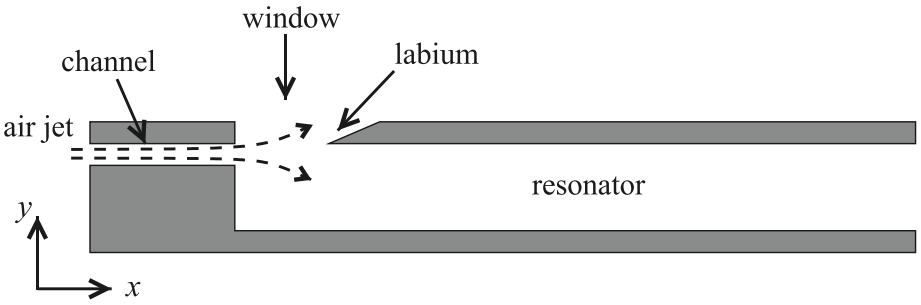

FIG. 1. Schematic of a recorder. The z direction is perpendicular to the page. For simplicity, tone holes have been omitted.

from the channel and impinges on and interacts with the labium edge can modify and suppress the half-harmonics.

II. THE INSTRUMENTS

Our experiments employed the Yamaha YRS-23 soprano recorder (Yamaha Corporation of America, Buena Park, CA) and a very similar instrument in which the tapered body of the YRS-23 is replaced by a cylindrical tube without tone holes. The YRS-23 is a student instrument; with all tone holes closed and at normal blowing pressures, it produces the note C5 (an octave above "middle C") with a fundamental frequency of approximately 523 Hz. This note will be the focus of our work though we have seen very similar half-harmonics for the note C6 played by these instruments; some results for that note will be given in the supplementary materials associated with this paper and accessible at the JASA website (Ref. 15, Sec. A). The YRS recorder has an air channel that is about 10 mm wide (along the z direction in Fig. 1) and 1.0 mm tall (in the y direction), with a chamfer at the outlet on the bottom edge. The length of the window region, i.e., the distance between the outlet of the channel and the tip of the labium, is approximately 3.5 mm. The section of the recorder "head" that extends from the outlet of the channel to the point where it connects to the body of the recorder has a length of about 6.0 cm. The full resonator (measured from the exit of the channel to the open end) is 28.3 cm long, and has an inside diameter that tapers from about 14 mm near the downstream end of the labium to around 8.8 mm at the open end.

For many of the results reported below, we replaced the tapered YRS resonator (length 22.3 cm) with a uniform cylindrical chlorinated polyvinyl chloride (CPVC) tube of length 24.4 cm and inside diameter of 12 mm. We will refer to this instrument as the CPVC instrument or simply the "cylindrical recorder" to distinguish it from the YRS recorder with its tapered body [which we will also refer to as the "tapered (YRS) instrument"]. The key point here is that the two different instruments have heads with the *same* dimensions, and differ only in their resonator geometries.

At low blowing pressures, the cylindrical recorder and the YRS recorder with all tone holes closed produce the note C5, with a fundamental frequency (dominant spectral component in the power spectrum) that we will denote as f_1. If the cylindrical recorder and the YRS recorder with all tone holes closed are both blown with sufficiently high pressures, they produce the note C6 having a dominant spectral component we will denote as f_2. These two notes are nominally an octave apart, with $f_1 \approx 523$ Hz and f_2 approximately equal to $2 \times f_1$. Also, as commonly found in wind instruments, our measured and simulated values of f_1 and f_2 increase slightly with blowing pressure, as will be seen in the examples below. In addition to observing the spectra of the notes C5 and C6 when the two instruments are blown, we have also measured the passive resonance spectra using a method developed by one of us.[16] The method uses a weak broadband (pink noise) source to excite the instrument while measuring the sound spectrum inside the instrument. Dividing the measured spectrum by the source spectrum yields the passive resonance spectrum. For a recorder, one expects the frequency of the played fundamental (f_1) to be near the frequency of the lowest peak in the passive resonance spectrum. One also expects the peaks in the passive resonance spectrum to be spaced approximately harmonically with respect to f_1. Such behavior was indeed found for both the cylinder model and the YRS model, and these spectra will be shown below. Denoting the first two peaks in the passive resonance spectrum as $f_1(passive)$ and $f_2(passive)$, we found $f_2(passive) - 2 \times f_1(passive) \approx -70$ cents (a compressed octave) for the cylinder model, and $f_2(passive) - 2 \times f_1(passive) \approx +30$ cents (a stretched octave) for the YRS model. One reason for studying the behavior of these two different instruments is to determine the effect, if any, of the different resonator shapes (cylindrical versus tapered) and harmonicity on the behavior of the half-harmonics.

The simulations used computer models with geometries similar to the cylindrical recorder and the YRS recorder. The dimensions of the computer models were similar to the physical instruments, but we made no attempt to exactly copy the complex geometry of YRS head and the transition region that connects to the circular cross section of the resonator. For this reason, we do not expect precise quantitative agreement between the experimental results and the simulations. However, we will find good qualitative agreement with essentially all of the experimental results.

We also explored, in both the experiments and simulations, the effect of modifications to the window region of both recorder models. These modifications consisted of a narrow post (1 mm wide) positioned in the window region, oriented parallel to the y direction in Fig. 1. The behavior with two different post positions was explored. In one case, the post was at the outlet of the channel and in the other, it was located midway between the exit of the channel and the

https://doi.org/10.1121/10.0022327

edge of the labium. In both cases, the post was in the middle of the window as viewed from the *y*–*z* plane in Fig. 1. Sketches of these geometries will be given in Sec. VII.

III. EXPERIMENTAL METHOD

The experimental setup, shown schematically in Fig. 2, consisted of the soprano recorder being tested, an artificial blower apparatus to make the instrument play, and a computer-connected external microphone to record the resulting audio signal.

The artificial blower apparatus was powered by a "whisper quiet" 40 lpm linear diaphragm pump (Hakko HK40L, Hakko Air Pumps, Laguna Hills, CA) whose output was fed through a home-built, balloon-based pulsation dampener to reduce the 120 Hz noise in the pump output. To reduce background noise, the pump was in one room and the recorder and microphone were in another. Two bleed valves (one coarse and one fine, both vented to the room with the pump) were used to manually adjust the flow, measured downstream by a digital gas mass flow meter (TSI/Alnor 5200 series, TSI, Inc., Shoreview, MN). The pressure at the input to the recorder was measured with one or two Magnehelic gauges (Dwyer, Michigan City, IN) with ranges 0–6.0 and/or 0–50 mm H_2O.

A USB-output cardioid pattern condenser microphone (AT2020, Audio Technica U.S. Inc., Stow, OH) was located about 20–30 cm from the recorder window. Sound files were recorded at a 44.1 kHz sampling rate with a laptop computer equipped with a real-time spectrum analyzer (Overtone Analyzer Live, Sygyt Software, Bochum, Germany). Data were collected at both fixed blowing pressures and as the blowing pressure was ramped up or down in a stepwise fashion at rates slow enough to maintain steady-state behavior. Sound power spectra were computed with a fast Fourier transform (FFT) algorithm (Audacity, audacityteam.org) using a 16 384 point FFT with a Hann window; sample lengths were typically 11–12 s for instrument configurations without the post and somewhat shorter (1.5–10 s) for the instrument configurations of Sec. VII with the post. Noise from the air source was typically visible at 60 and 120 Hz but could always be distinguished from the spectral features produced by the instrument.

IV. SIMULATION METHOD

The simulations used an explicit finite difference algorithm[17] to numerically solve the compressible Navier–Stokes equations, using values for the density, speed of sound, and kinematic viscosity for air. An artificial viscosity term was used to suppress instabilities,[18] but no other smoothing or filtering was applied. This algorithmic approach is second order accurate in both space and time; it is well tested and has been used successfully (and described at length) in modeling studies of several different wind instruments.[19–22] We note that a recent study of regime change in the recorder with instrument geometries similar to those studied in this paper[13] found good quantitative agreement between the simulations and experiments.

Our use of the Navier–Stokes equations as the basis for our simulations means that there are no unknown parameters of the kind inherent in lumped models.[23] The feedback from the labium to the air jet as it emerges from the channel, the coupling of the air jet to the resonator, etc., are all accounted for "automatically" in the Navier–Stokes equations. In our simulations, we specify the speed of the air jet in the initial few millimeters at the inlet end of the channel[19] as the control parameter that determines how "hard" the instrument is blown. (This differs from the experiments in which the pressure just upstream from the entrance to the channel is the corresponding

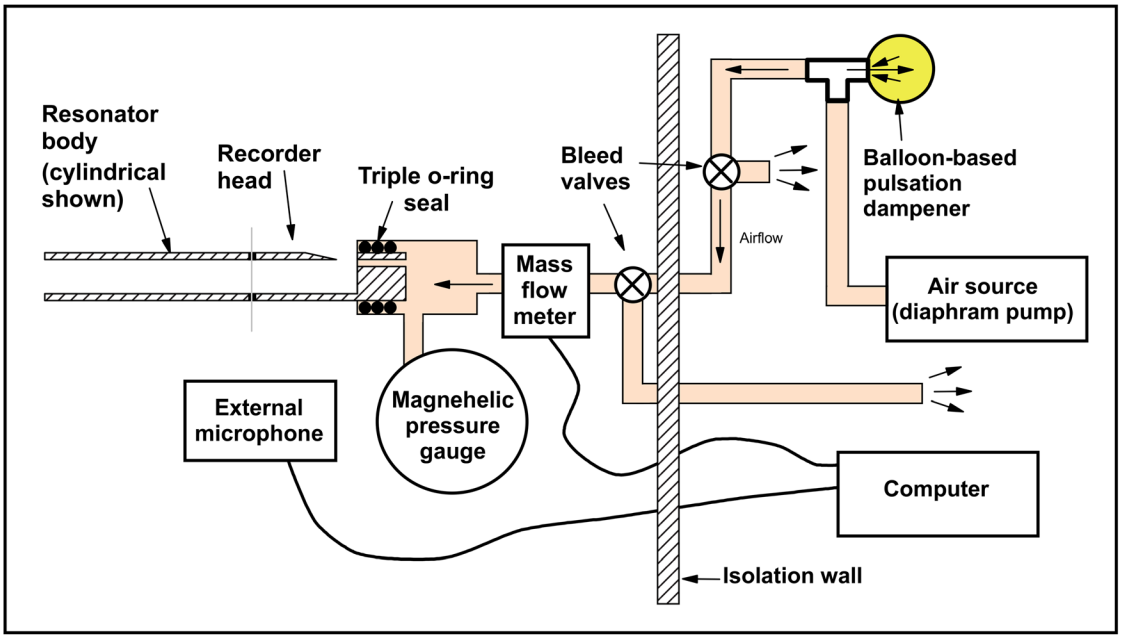

FIG. 2. (Color online) Schematic of the experimental apparatus.

control parameter.) This means that, unlike in the experiments, there is no mouth cavity upstream from the recorder channel, so pressure oscillations in that upstream region can play no role in the behavior in the simulations. However, pressure oscillations will still be present in the channel due to changes in the pressure and flow in the window region.

In the simulation results reported below, the blowing speed at the entrance to the channel was generally held fixed long enough to reach steady state (typically 0.2 s or longer), at which time, the spectrum of the sound power outside the instrument (typically a few tens of cm away from either the open end or the window region) was computed. The calculations of the spectra for the simulations used Fourier transforms of typically 0.4 s of data recorded at 22 kHz and were computed with a Hann window with 8192 points.

Since the precise geometry of the window region in the simulation model was not identical to that of the actual YRS recorder head and the blowing in the simulations did not involve a mouth cavity, we should not expect perfect agreement between the experiments and the simulations. However, the similarity of so many key features in the results allow us to use the simulations to probe issues that are difficult to address with the experiments and vice versa.

V. CYLINDER MODEL

We begin with the experimental results for the cylindrical recorder model. Figure 3 shows the waveform of the sound signal as a function of time (top panel) and a spectrogram of this signal showing the variation of the spectrum over the same time interval (bottom panel). Here, the blowing pressure was increased in a stepwise fashion, with the values of the mouth pressure (i.e., the pressure upstream from the recorder) indicated in units of Pa in the top panel and the associated speed of the air jet given in the caption. The initial pressure is approximately the lowest value that gives an audible C5 tone and the highest pressure is in the range that the tone has transitioned from C5 to the note an octave higher (C6). In the C5 region, the dominant spectral component has a frequency of about $f_1 = 523$ Hz and is accompanied by weaker integer harmonics. In the C6 region, the dominant spectral component has a frequency f_2 that is *approximately* twice f_1, with strong components at integer multiples of f_2 present at the highest pressures. As discussed previously,[13] there are additional spectral components that appear as combination tones or "sidebands" around the integer harmonics in the transition region around $p = 140$ Pa, where both f_1 and f_2 are strong. We hope to report more on these harmonics and their sidebands in the future. At present, we only note that (1) the frequencies f_1 and f_2 do not form a "perfect" octave, i.e., f_2 is significantly smaller than $2 \times f_1$, and (2) the combination tones appear to have frequencies given approximately by sums and differences of integer multiples of f_1 and f_2, with frequency spacings of $f_2 - 2 \times f_1$. This suggest that the sidebands are produced by the nonlinear mixing of components with base frequencies f_1 and f_2.

In this paper, we will focus on the behavior in the C5 region, the region at blowing pressures below about 120 Pa in Fig. 3, where a number of half-harmonic components are indicated in the spectrogram. The half-harmonics are most apparent in the pressure range 70–100 Pa; the solid curve in Fig. 4 shows the sound power spectrum at $p \approx 80$ Pa. The peak sound power of the half-integer harmonic of order $\frac{1}{2}$ is about 5 orders of magnitude smaller than that of the fundamental (f_1). At this blowing pressure, the sound powers of the half–harmonics are roughly constant over the 0–2000 Hz frequency range shown.

The dotted curve at the bottom in Fig. 4 is proportional to the passive resonance spectrum measured for this instrument using the method developed by one of us.[16] [See

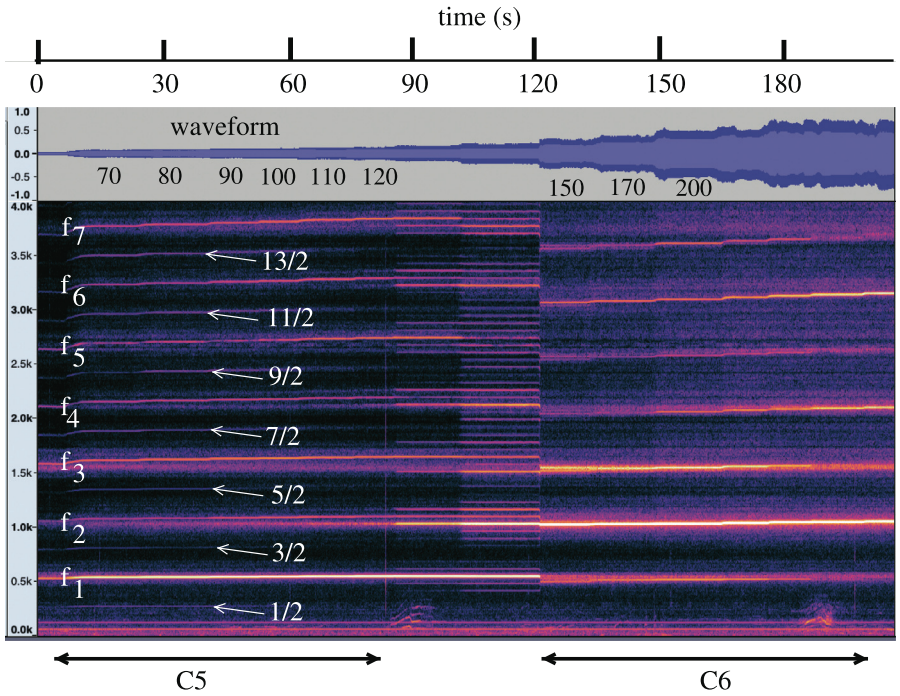

FIG. 3. Spectrogram measured experimentally for the cylinder model. Time varies along the horizontal axis (top) with the waveform of the sound signal shown in the top panel, and the magnitude of the sound power indicated in the spectrogram below. The numbers in the waveform panel give the pressure upstream of the channel in Pa; values of this pressure are given at several times, but not all pressure changes and values are indicated. Air jet speeds (estimated using the measured flow rate and the 0.1 cm^2 channel exit area) vary from 6.1 m/s at $p = 70$ Pa, to 8.7 m/s at 120 Pa, 11.0 m/s at 170 Pa, and 12.2 m/s at 200 Pa. Integer and half-integer harmonics in the C5 region are indicated. The pump noise mentioned in the text is visible at 60 and 120 Hz. The noise spikes around $t = 90$ and 185 s were caused by acoustic disturbances from outside the lab.

https://doi.org/10.1121/10.0022327

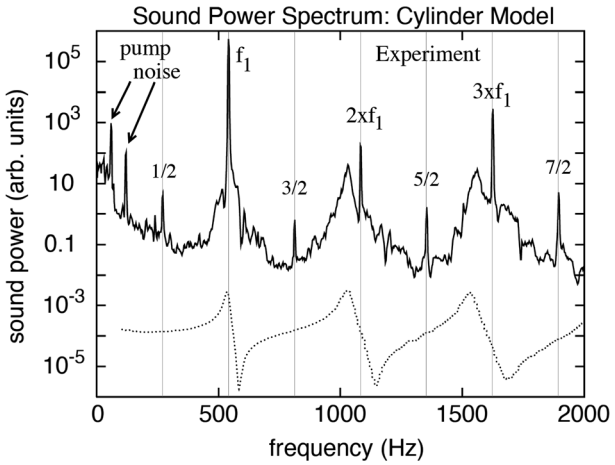

FIG. 4. Solid curve: Sound power spectrum measured for the cylinder model with a blowing pressure of 80 Pa and an air jet speed (estimated using the measured flow rate and the 0.1 cm^2 channel exit area) of 6.7 m/s. The integer harmonics are indicated as f_1, $2 \times f_1$, etc., and the half-harmonics by $\frac{1}{2}$, $\frac{3}{2}$, etc. Here, and in all of the simulation spectra shown in the following figures, each tick mark on the vertical axis corresponds to an order of magnitude change in the sound power in arbitrary units. Dotted curve: Passive resonance spectrum with the data shifted along the vertical. The thin vertical lines are positioned at frequencies equal to f_1 (as determined by the peak in the sound power spectrum) and multiples (integer and half-integer) of f_1.

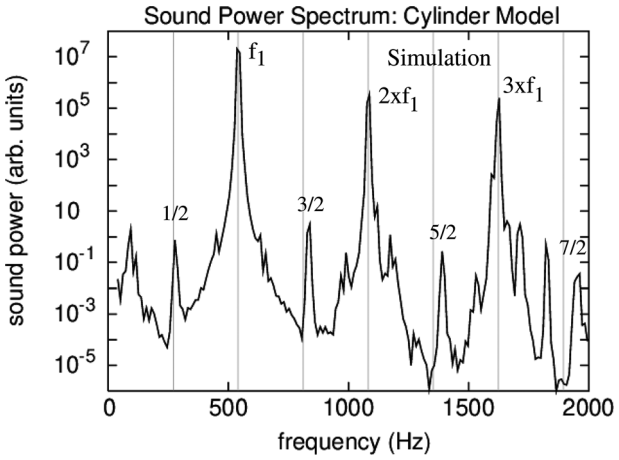

FIG. 5. Sound power spectrum from a simulation of the C5 cylinder model with an air jet speed (estimated using the measured flow rate and the 0.1 cm^2 channel exit area) of 7.1 m/s. Several harmonics and half-harmonics are indicated. The thin vertical lines are positioned at frequencies equal to f_1 (as determined by the peak in the sound power spectrum of the simulation) and multiples (integer and half-integer) of f_1.

supplementary (Ref. 15, Sec. B) for details on the experimental geometry.] As explained in Ref. 16, the peaks in the dotted curve give the positions of the passive resonances. As expected, the $n = 1$ (played) harmonic at f_1 is seen to be nearly coincident with the lowest passive resonance at approximately 535 Hz [denoted in Sec. II by $f_1(passive)$]. The second and third peaks in the passive resonance spectrum, which lie at $f_2(passive) \approx 1030$ Hz and $f_3(passive) \approx 1540$ Hz, are well aligned with broad peaks in the played spectrum but are clearly below the corresponding played frequencies at $2 \times f_1$ at $3 \times f_1$. We believe that these broad peaks in the played spectrum are a result of these underlying passive resonances.

The simulation results for the cylinder model are considered next. Figure 5 shows a simulation in which the blowing speed was held fixed in the C5 region. While the half-integer harmonics are several orders of magnitude smaller in magnitude than the neighboring integer harmonics, they are unmistakable. There are also additional peaks between the integer harmonics (the largest in Fig. 5 being above $3 \times f_1$), which we will discuss below. We suspect that some of these may have an origin similar to the sidebands seen in the experimental results in Fig. 3, but in some cases, they appear to have frequencies corresponding to subharmonics of order $\frac{1}{4}$ and $\frac{3}{4}$. We will return to this possibility below in connection with the simulation results for the YRS model.

The spectrum from the simulation in Fig. 5 is similar, but certainly not identical, to the experimental spectrum in Fig. 4. For example, the half-harmonic of order $\frac{1}{2}$ in the simulation is about 7 orders of magnitude smaller than the harmonic at f_1, while in the experiment the half-harmonic of order $\frac{1}{2}$ is nearly 5 orders of magnitude smaller than the harmonic at f_1. In addition, in the simulation, the harmonic of order $\frac{3}{2}$ is larger than the harmonic of order $\frac{1}{2}$, while in the experiment, the $\frac{3}{2}$ harmonic is smaller than the harmonic of order $\frac{1}{2}$. As noted in Sec. II, we do not expect perfect quantitative agreement since the geometry of model in the vicinity of the window and labium are similar but not identical to those of the real instrument. With this caveat, we believe that nearly all of the major features seen in the experiments are found also in the simulation. One small and perhaps important difference between the results in Figs. 4 and 5 involves the precise locations of the frequencies of the half-harmonics. In the experiments, the half-harmonic frequencies are, to within the spectral resolution, precisely midway between the integer harmonics. In the cylinder model simulations, the frequency of the half-harmonic of order $^1/_2$ (which can be denoted as $f_{1/2}$) is slightly above $f_1/2$, and other half-harmonics are (to within the uncertainties) exactly equal to odd integer multiples of $f_{1/2}$. In Fig. 5, this is quite noticeable, as the half-harmonics are systematically higher in frequency than the corresponding half-integer multiples of f_1. This behavior is *not* found in simulations for the YRS model (below), and while this result is not understood, it does suggest that for this model geometry, the half-integer harmonics could have an origin distinct from period doubling, or that they are affected somehow by some aspect of the instrument geometry. In any case, this may be a useful clue in learning more about the origin of the half-harmonics.

VI. YRS MODEL

Results for the YRS model are shown in Fig. 6 (the experiments) and Fig. 7 (the simulation). In both cases, the blowing pressure and speed were in the range that produces a C5 tone, and in both cases, half-harmonics are clearly visible. As with the cylinder model, the relative magnitude of the half-harmonic $f_{1/2}$ (i.e., the spectral power at $f_{1/2}$ compared to the power at f_1) found experimentally is still significantly larger than found in the simulations, though the

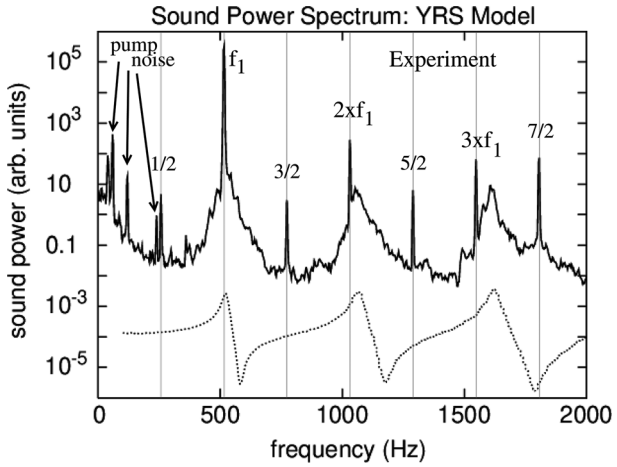

FIG. 6. Solid curve: Sound power spectrum found experimentally for the YRS model, with labels as in Fig. 4. The blowing pressure was 60 Pa and the air jet speed (estimated using the measured flow rate and the 0.1 cm^2 channel exit area) was 5.9 m/s. Dotted curve: Passive resonance spectrum, shifted vertically for clarity. The thin vertical lines are positioned at frequencies equal to f_1 (as determined by the peak in the sound power spectrum) and multiples (integer and half-integer) of f_1.

discrepancy between experiment and simulation for the YRS is now only 1 order of magnitude (versus nearly 2 orders of magnitude for the cylinder).

One interesting feature in the simulation results in Fig. 7 is the appearance of peaks at frequencies $[(1/4)+n]f_1$ and $[(3/4)+n]f_1$ for $n=0,\,1,2,3$. This suggests the possibility that a second period doubling bifurcation may have occurred.[3]

The results for the YRS model (Figs. 6 and 7) are thus very similar to those for the cylinder model (Figs. 4 and 5), with both clearly exhibiting half-integer harmonics. However, in contrast with the simulations of the cylinder model, the frequencies of the half-harmonics in the YRS simulation are, to within the spectral resolution, exactly midway between the integer harmonics. It is also worth

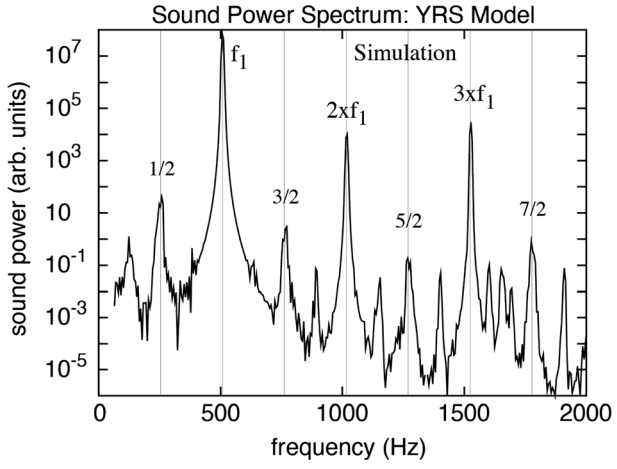

FIG. 7. Sound power spectrum found in the simulation for the YRS model. The air jet speed was 8.5 m/s. The thin vertical lines are positioned at frequencies equal to f_1 (as determined by the peak in the sound power spectrum of the simulation) and multiples (integer and half-integer) of f_1.

noting that the presence of harmonics of order $\frac{1}{4}$ and $\frac{3}{4}$ in the YRS simulation (again with the expected frequencies, to within the uncertainties) would seemingly rule out an explanation considered for the half-integer harmonics, namely, that some geometrical aspect of channel/window/labium end of the resonator gives rise to some residual behaviors characteristic of a closed input (versus one treated as fully open). Modes from a resonator acting as a tube that is open at one end and closed at the other, should they occur together with the usual modes of a resonator open at both ends, could conceivably lead to modes with the frequencies of the observed half-integer harmonics. However, it is hard to see how such modes would give rise to harmonics of order $\frac{1}{4}$ and $\frac{3}{4}$. Furthermore, a resonator having an end geometry that is simultaneously open and closed would appear to be inconsistent with all conventional understandings of boundary conditions in wind instruments.

VII. POSSIBLE ORIGIN OF THE FRACTIONAL HARMONICS AND COMBINATION TONES

Many oscillatory systems possess a spectrum dominated by a single spectral peak. If the associated oscillations are not perfectly sinusoidal, there will also be additional spectral components whose frequencies follow a pattern nf_1 where n is an integer. In addition, when an oscillatory system contains nonlinearities, it is often found that different modes of oscillation can combine to produce sum and difference frequencies. In this way, a musical instrument can exhibit a spectrum that contains many different spectral components (e.g., Ref. 24). However, such nonlinearities usually only produce frequencies that are sums or differences of integer multiples of two or more base frequencies. To the best of our knowledge, the only mechanism that can produce the half and quarter fractional harmonics of the kind observed in Figs. 4–7 is that found in nonlinear dynamical systems.[3,4] The period doubling route to chaos is a well-studied case that leads to half-integer harmonics, and the mathematical ingredients necessary in the relevant equations of motion to give such behavior are also well known. For a system, such as the recorder, an obvious candidate for this mechanism is the fluid dynamic interaction of the air jet as it emerges from the channel and interacts with the labium. This reasoning led us to conduct studies in which the trajectory of the air jet and its interaction with the labium are modified by changes to the geometry in the vicinity of the window and labium. We next describe the results for two of these geometries, which are shown schematically in Fig. 8. We will refer to the geometry in Fig. 8(a) as the channel post model; in this case, a narrow post is positioned against the outlet of the channel. We will refer to the geometry in Fig. 8(b) as the window post model; here, a longer post is positioned at the center of the window region, midway between channel outlet and the labium. In both cases, the posts were in the center of the channel as viewed along the z direction, perpendicular to the plane of the figure. For the experiments, the post was formed from a cylindrical 1.1 mm–diameter hypodermic tube, bent to form a rounded

https://doi.org/10.1121/10.0022327

(90°) bend between two 22 mm–long straight sections, with one section used as the obstruction and the other used as a handle. For the post at the channel position, the bottom end of the section used as the obstruction was in contact with the chamfer [as shown in Fig. 8(a)]; for the post at the window center, the bottom end of the section used as the obstruction was about 4–5 mm below the top of the channel. For the simulations, the post had a square, $1 \times 0.5\,\text{mm}^2$ cross section (as viewed in the x–z plane) and extended from the top of channel to the chamfer. Hence, in both cases, the post was much narrower than the width of the channel along the z direction (which was approximately 10 mm; the height of the channel, along y was approximately 1.0 mm). The effects of the posts were investigated using experiments and simulations, for both the cylindrical and YRS (tapered) resonators.

Figure 9 shows a comparison of the experimental behavior of the cylinder model with a post at the outlet of the channel with the behavior of the unmodified instrument. The presence of the post greatly suppresses the half-integer harmonics while leaving integer harmonics (frequencies nf_1 with n an integer) relatively unchanged. Also shown in the supplementary material (Ref. 15, Sec. C) is a comparison of the experimental results for the cylinder model with the post in the two positions (at the channel outlet and at the center of the window) again compared with the unmodified instrument. Placing the post in the center of the window reduces the half-integer harmonics, but not as much as found when the post is at the channel outlet. Similar experimental results were found for the tapered (YRS model) C5 and cylindrical C6, as shown in Ref. 15, Secs. D and E.

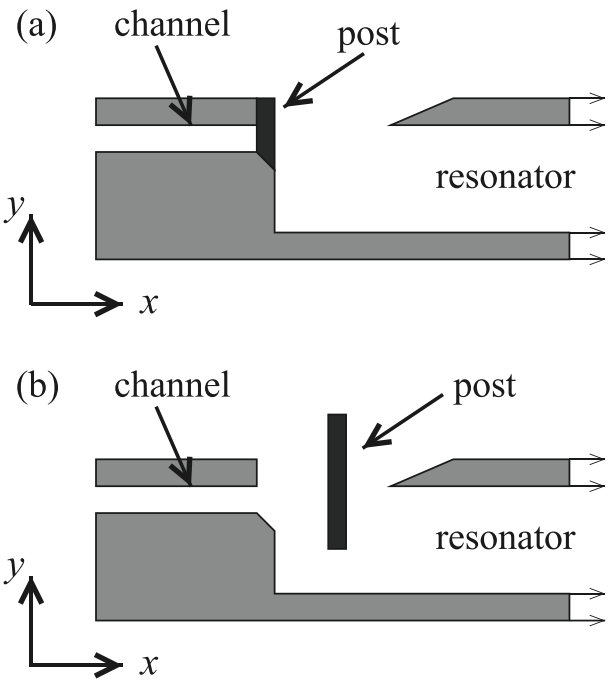

FIG. 8. Modifications of the recorder geometry studied in this work. The window region was modified with posts inserted between the channel and labium. These sketches are not to scale. In both cases, the width of the post (along the z direction) was approximately 1 mm. (a) Side view of the channel post model in which a post is located at outlet of the channel. This sketch shows the geometry of the simulation model. For the experiment, the post extended several millimeters above the top of the instrument. (b) Side view of the window post model in which a post is located at the center of the window region. The z direction mentioned here and in the text is perpendicular to the plane of the drawings.

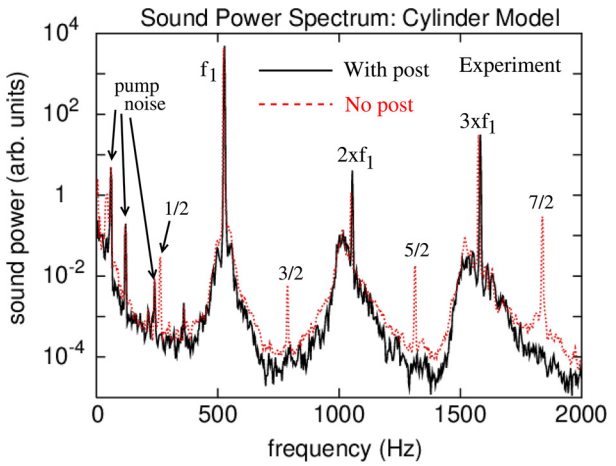

FIG. 9. (Color online) Solid curve: Experimental sound power spectrum for the cylinder model with a post at the outlet of the channel. Dotted curve: Experimental results for the unmodified instrument. For both results, the blowing pressure was 60 Pa and the jet speed was 5.9 m/s.

Figure 10 gives simulation results for the cylinder model and shows that placing the post at the channel outlet almost completely suppresses the half-integer harmonics while leaving the integer harmonics relatively unchanged. Some of the prominent sidebands around the integer harmonics are also suppressed by the post. Results available in the supplementary material (Ref. 15, Sec. C) show simulation results for the cylinder model with the post in the two positions (at the channel outlet and at the center of the window) compared with the unmodified instrument. For this blowing speed, placing the post in the center of the window reduces the half-integer harmonics by essentially as much as found when the post is at the channel outlet.

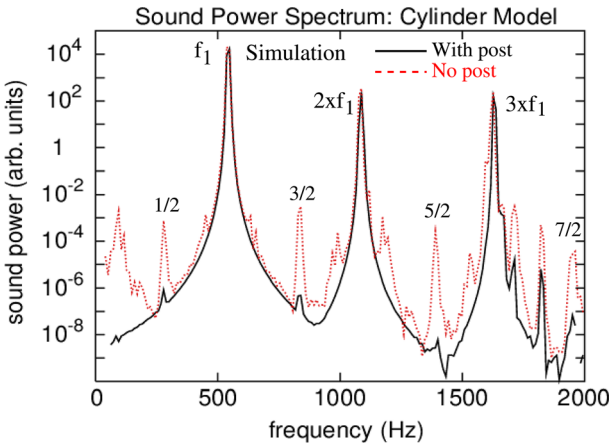

FIG. 10. (Color online) Solid curve: Simulated sound power spectrum for the cylinder model with a post at the outlet of the channel. Dotted curve: Simulation results for the unmodified instrument. For both results, the jet speed was 7.1 m/s.

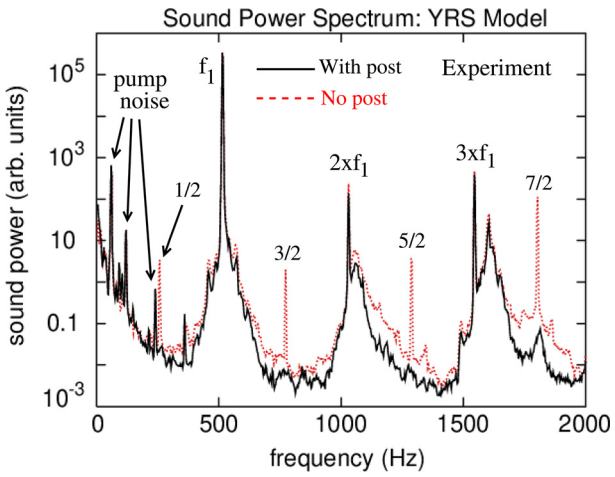

FIG. 11. (Color online) Solid curve: Experimental sound power spectrum for the YRS model with a post at the outlet of the channel. Dotted curve: Experimental results for the unmodified instrument. For both cases, the blowing pressure was 60 Pa and the air jet speed was 5.9 m/s.

The experimental and simulation results for the cylinder model both show that the addition of a post in the channel/window region suppresses the half-integer harmonics in both the experiments and the simulations. A similar result is found for the YRS model; experimental results for that model are shown in Fig. 11, with the corresponding simulations in Fig. 12. The fact that the posts suppress the half-integer harmonics in a very similar way with the different resonators in the two models (cylindrical versus tapered) again suggests that the half-integer harmonics originate in the window/labium region. Experiments in which the post was positioned at other locations in the window region also found a suppression of the half-integer harmonics, with the degree of suppression depending on the location of the post and the geometry of the resonator. In addition, experiments showed that (1) adding a thin (1 mm) layer of material to the top surface of the labium, and (2) blowing a second air jet

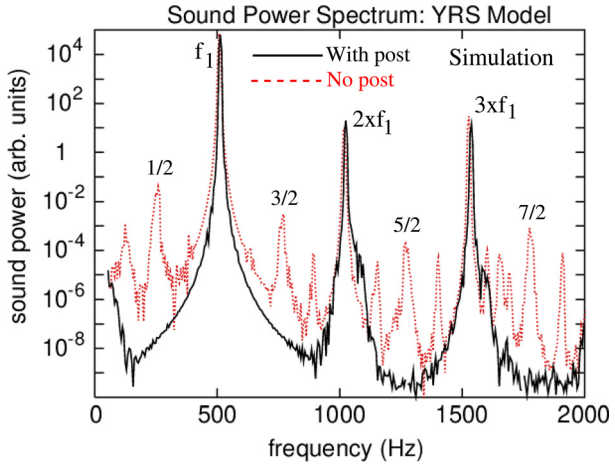

FIG. 12. (Color online) Solid curve: Simulated sound power spectrum for the YRS model with a post at the outlet of the channel. Dotted curve: Simulation results for the unmodified instrument. For both cases, the air jet speed was 8.5 m/s.

across the top of the labium (jet diameter approximately 6 mm, positioned a few millimeters downstream from the edge) both suppressed the half-integer harmonics. These results suggest that the interaction of the jet with the labium, and the way the jet flows over the top of the labium, and not just the modification of the air jet as it exits the channel, play an important role in suppressing the half-integer harmonics. We expect that other changes that affect the flow pattern will suppress the half-harmonics in a similar way.

The results for the cylinder and YRS models in Figs. 9–12 show that the presence of the post has a profound effect on the half-integer harmonics. However, given the low intensities of these half-harmonics, one might wonder if they are audible. Experimentally, one finds distinct differences in perceived tone quality upon sequential switching between various post positions. An audio file of such a sequence is provided in the supplementary material (Ref. 15, Sec. F) for the case of the tapered instrument. The half-harmonics are clearly associated with a faint buzzing sound.

It is also worth noting that the presence of the post seems to reduce the spectral background in the vicinity of the half-integer peaks for the C5 data shown here. The reduction is especially noticeable in the simulations for the YRS model (Fig. 12). It is tempting to attribute this background to "turbulence noise" and somewhat surprising that the post would decrease such noise.

VIII. FLOW PATTERNS

To this point in the present paper, the main use of the simulations has been as a comparison with the experimental results, and we have found good overall agreement for the main spectral features of the different models. This agreement means that the simulations are able to capture the physical mechanism(s) responsible for the half-integer harmonics. In this section, we want to consider an aspect of the behavior that is most readily accessible in the simulations: the details of the flow patterns near the labium. We are particularly interested in how the flow patterns might be different in cases that do or do not contain modifications of the channel/window region; i.e., that do or do not exhibit fractional harmonics.

The simulations yield the complete flow information, i.e., the values of the density and the three components of the velocity vector, as functions of position and time. These results can be used to produce images of the flow in various ways. In previous work by Giordano,[19] such results have typically been displayed as snapshots of the density and flow speed in a plane that cuts through the middle of the labium and resonator, i.e., the x–y plane in Fig. 1. In this paper, we will consider images of the flow in three-dimensional renderings of the streamlines that emerge from the channel as air flows around the labium.[25–28] Data files showing movies of these streamlines over complete oscillation cycles can be found in the supplementary material (Ref. 15, Sec. G). Figs. 13 and 14 show selected frames from movies produced from the simulations used to obtain the

https://doi.org/10.1121/10.0022327

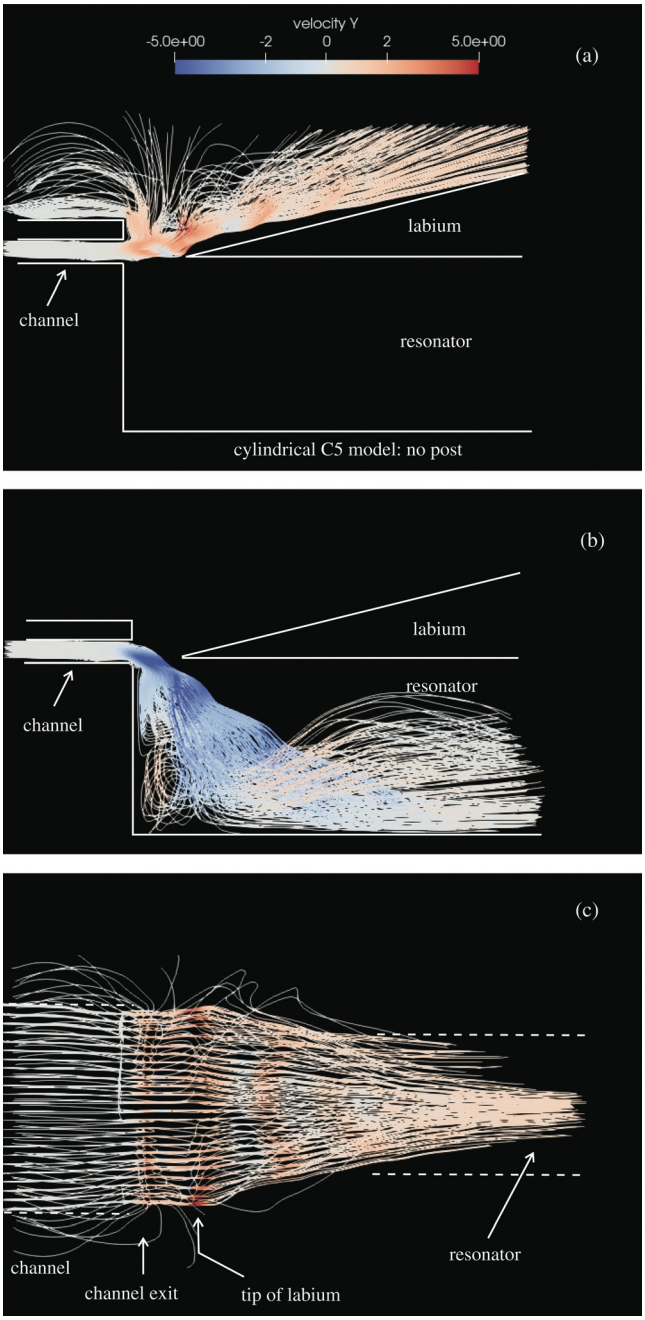

FIG. 13. Images of streamlines obtained from simulations of the cylinder model with an unmodified labium/channel, with an air jet speed of 7.1 m/s. The spectrum in Fig. 5 was obtained from this simulation. (a) Side view (as in Fig. 1) at a time when the air jet passes above the labium. The solid white lines show the approximate edges of the channel, labium, and resonator. The color of each streamline is determined by the component of the velocity along the y (vertical) direction. Note that as the streamlines pass over the tip of the labium, they are deflected somewhat above the surface of the labium as indicated by the absence of streamlines just above the upper edge of the labium. (b) Side view showing streamlines at a later time in an oscillation cycle when the air jet trajectory is mainly into the resonator. (c) View looking down from above the labium; i.e., looking along the $-y$ direction in Fig. 1, showing the flow as it leaves the channel and passes over the labium. The edges of the channel are shown as dashed lines. This image shows the streamlines at the same instant as the image in part (a) was recorded, so these streamlines pass "above" the labium and essentially no streamlines enter the resonator, whose edges (which are *below* the labium) are shown dashed lines.

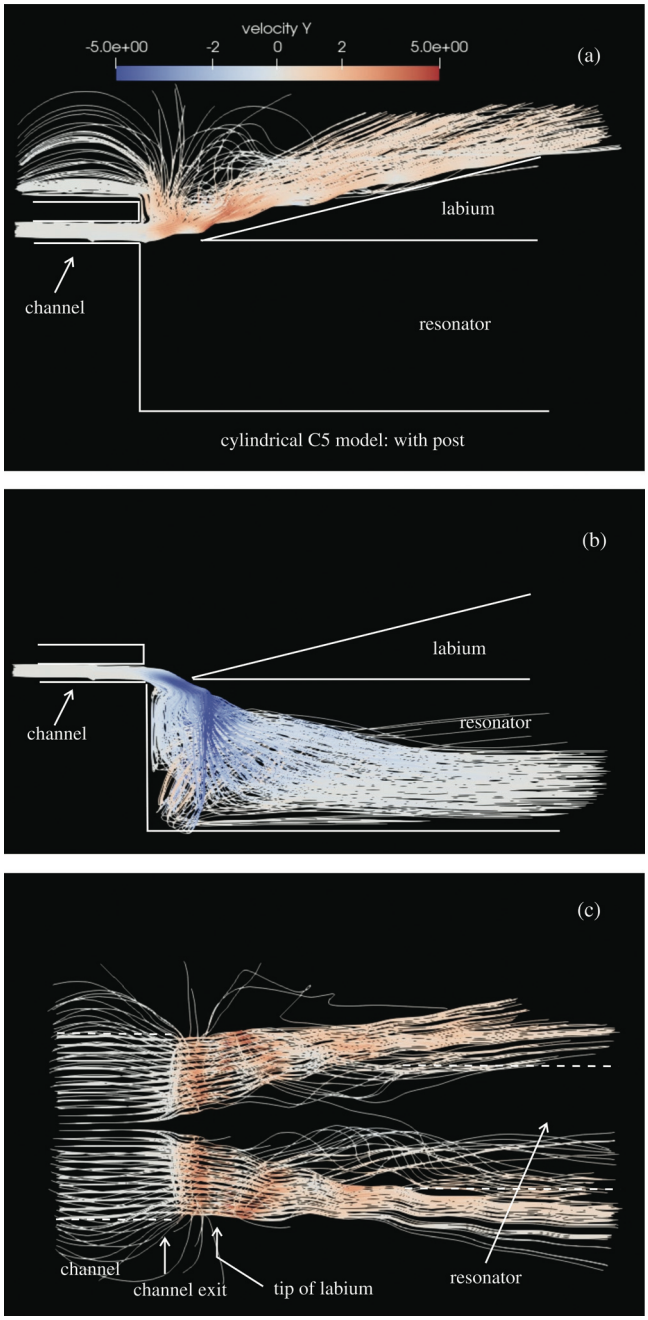

FIG. 14. Images of streamlines obtained from simulations of the cylinder model with a post at the outlet of the channel [Fig. 8(a)] with an air jet speed of 7.1 m/s. Parts (a), (b), (c) are structured and annotated as in the corresponding parts of Fig. 13. (a) Side view at a time when the air jet passes above the labium. (b) Side view showing streamlines at a later time in an oscillation cycle when the air jet trajectory is mainly into the resonator. (c) View looking down from above the labium; i.e., looking along the $-y$ direction in Fig. 1, showing the flow as it leaves the channel and passes over the labium.

spectra (Fig. 10) for the cylinder model with and without a post at the outlet of the channel.

We begin with the three images in Fig. 13 showing the flow trajectories for the unmodified cylinder model. Figures 13(a) and 13(b) are views from the side of the channel (the same perspective as in Fig. 1) at two different moments in an oscillation cycle. Figure 13(c) shows the streamlines as

viewed looking down on the window region from above in Fig. 1, at the same instant as the side view image was captured in part (a) of the figure. These streamlines were calculated from starting points in the inlet region of the channel and the colors of the lines are determined from the flow velocity along the y direction (perpendicular to the long edge of the labium) in Fig. 1. In our initial discussion of Fig. 1, we stated that under normal playing conditions, the air jet oscillates between trajectories above and below the labium. Figure 13(a) shows the streamlines when this trajectory is above the labium; hence, the vast majority of streamlines that emanate from the channel are above the labium. As noted above, the color of a streamline is based on the flow velocity along the y direction, which is why the streamlines in the channel are white ($v_y \approx 0$) while the streamlines above the labium are tinted orange/red ($v_y > 0$). Figure 13(b) shows the streamlines somewhat later in an oscillation cycle, when the flow is mainly below the labium and into the resonator. Now many of the streamlines are blue as they emerge from the channel, corresponding to $v_y < 0$, with the color then changing to white and/or red as one moves farther into the resonator.

Figure 13(c) shows a third image of the streamlines from the same simulation, but now as viewed from the perspective of a point above the channel, window, and labium. The net flow is again from left to right. The dashed lines on the right in Fig. 13(c) show the interior edges of the cylindrical resonator to show the overall scale, even though these edges are *inside* the instrument while these streamlines in this image are *above* the labium. The white streamlines on the far left in Fig. 13(c) are in the channel and are white since $v_y \approx 0$ in that region. As the streamlines emerge from the channel in Fig. 13(c), they are red in color, since $v_y > 0$ as these streamlines travel over the top of the labium. An interesting and unexpected feature in that region is that these streamlines concentrate toward the *center* of the labium as the air moves downstream along and over the top of the labium. This region is *above and outside* the resonator. In the simulation model, there are no solid walls along the sides of the labium (as shown in Fig. 1 of Ref. 13) to cause this narrowing of the flow; it must be due to a purely aerodynamic effect.

We next consider the behavior of the streamlines in the cylinder model containing a post at the channel outlet. Figure 14 shows three images, which are similar in perspective and time during an oscillation cycle to the images in Fig. 13. Figures 14(a) and 14(b) show a side view of the streamlines at two different times in an oscillation cycle and Fig. 14(c) shows the streamlines looking down on the window region from above. The side views in Figs. 14(a) and 14(b) show the streamlines as they oscillate from trajectories above and below the labium, and resemble the corresponding images in Figs. 13(a) and 13(b) for the instrument without a post at the channel outlet. However, the streamlines in Fig. 14(c) are quite different from the image from the same perspective and without the post in Fig. 13(c). The streamlines in Fig. 14(c) split at the post and move apart as they flow away from the channel. That is, the air seems to *move away from* the central axis as it flows over and downstream from the labium, suggesting that the flow has concentrated at the lateral edges of the labium; i.e., the edges at large negative and positive z in Fig. 1.

The images of the flow in Figs. 13 and 14 show that the insertion of the post at the center of the channel outlet has a profound effect on the flow trajectories. Qualitatively, similar changes in the flow patterns were found with the post in the center of the window, although the changes in that case were somewhat smaller than with the post at the channel outlet. The presence of the post produces changes in the flow that are quite striking, and to the best of our knowledge, there is no theory or model, quantitative or qualitative, that explains these flow trajectories. Given the way in which the post suppresses the half-integer harmonics, it is certainly tempting to associate the flow patterns in Figs. 13 and 14 with the mechanism responsible for the half-harmonics.

IX. CONCLUSIONS

As noted in the Introduction, ours are not the first experimental observations of half-integer harmonics in the spectrum of a recorder. However, our ability to compare these observations with first principles (Navier–Stokes—based) modeling studies of very similar instrument geometries has yielded new insights into this behavior.

Our results strongly suggest that the half-harmonics are closely related to the air flow in the window region as it affects the interaction of the air jet with the labium. This is not surprising since it is well established that a strongly driven fluid can exhibit a period doubling route to chaos. The details of how such a description applies to the recorder remain to be elucidated, perhaps through an analysis involving bifurcation diagrams and Lyapunov exponents, or a much more sophisticated image analysis of the flow patterns, or both. Our results for the flow geometry as visualized through the streamlines in three dimensions are, so far as we know, also new, with the behavior of the streamlines for even the unmodified instrument (Fig. 13) raising interesting questions. These are problems that we leave for the future. It is amazing that an instrument as (apparently) simple as the recorder continues to provide surprises.

ACKNOWLEDGMENTS

We thank P. Rucz for some very useful conversations and private communications about his work on this problem. This work was supported in part by U.S. National Science Foundation Grant No. PHY1806231.

AUTHOR DECLARATIONS

Conflict of Interest

The authors have no conflicts of interest to disclose.

DATA AVAILABILITY

Additional data that support the findings of this study are available from the corresponding author upon reasonable request.

[1]A. Chaigne and J. Kergomard, *Acoustics of Musical Instruments* (Springer-Verlag, New York, 2016), Chap. 10..
[2]J. Angster, P. Rucz, and A. Miklós, "Acoustics of organ pipes and future trends in the research," Acoust. Today **13**(1), 10–18 (2017).
[3]M. J. Feigenbaum, "Quantitative universality for a class of nonlinear transformations," J. Stat. Phys. **19**, 25–52 (1978).
[4]G. B. Lubkin, "Period-doubling route to chaos shows universality," Phys. Today **34**(3), 17–19 (1981).
[5]T. Idogawa, T. Kobata, K. Komuro, and M. Kiwaki, "Nonlinear vibrations in the air column of a clarinet artificially blown," J. Acoust. Soc. Am. **93**, 540–551 (1993).
[6]T. D. Wilson and D. H. Keefe, "Characterizing the clarinet tone: Measurements of Lyapunov exponents, correlation dimension, and unsteadiness," J. Acoust. Soc. Am. **104**, 550–561 (1998).
[7]V. Gibiat and M. Castellengo, "Period doubling occurrences in wind musical instruments," Acta Acust. united Acust. **86**, 746–754 (2000).
[8]P.-A. Taillard, J. Kergomard, and F. Laloë, "Iterated map for clarinet-like systems," Nonlinear Dyn. **62**, 253–271 (2010).
[9]M.-P. Verge, "Aeroacoustics of confined jets, with applications to the physical modeling of recorder-like instruments," Ph.D. thesis, Technische Universiteit Eindhoven, Eindhoven, Netherlands, 1995.
[10]D. Ferrand, C. Vergez, B. Fabre, and F. Blanc, "High-precision regulation of a pressure controlled artificial mouth: The case of recorder-like instruments," Acta Acust. united Acust. **96**, 701–712 (2010).
[11]S. Terrien, C. Vergez, and B. Fabre, "Flute-like musical instruments: A toy model investigated through numerical continuation," J. Sound Vib. **332**, 3833–3848 (2013).
[12]P. Rucz, J. Angster, and A. Miklós, "Modulation and instability in the sound of plastic soprano recorders," J. Acoust. Soc. Am. **141**, 3960 (2017).
[13]N. Giordano, K. L. Saenger, and J. W. Thacker, "Study of hysteretic behavior in the recorder," Proc. Mtgs. Acoust. **49**, 035002 (2022).
[14]Z. Otčenášek, J. Otčenášek, and P. Dlask, "Changes of the air jet motion, tone spectra and perceived organ pipe sound caused by voicing adjustments," Proc. Mtgs. Acoust. **49**, 035024 (2022).
[15]See supplementary material at https://doi.org/10.1121/10.0022327 for Secs. A–G showing additional figures, tables, videos, and discussions omitted for space reasons.
[16]K. L. Saenger, "A pressure-based transfer matrix method and measurement technique for studying resonances in flutes and other open-input resonators," J. Acoust. Soc. Am. **147**, 2556–2569 (2020).
[17]R. W. MacCormack, "The effect of viscosity in hypervelocity impact cratering," in *AIAA Hypervelocity Impact Conference*, Cincinnati, OH (April 28–30, 1969), Paper 69–354, pp. 1–7.
[18]A. Jameson, W. Schmidt, and E. Turkel, "Numerical solution of the Euler equations by finite volume methods using Runge Kutta time stepping schemes," in *14th Fluid and Plasma Dynamics Conference*, Palo Alto, CA (June 23–25, 1981), Paper 81–1289, pp. 1–14.
[19]N. Giordano, "Simulation studies of a recorder in three dimensions," J. Acoust. Soc. Am. **135**, 906–916 (2014).
[20]N. Giordano, "Physical modeling of a conical lip reed instrument," J. Acoust. Soc. Am. **143**, 38–50 (2018).
[21]N. Giordano and J. W. Thacker, "Navier-Stokes-based model of the clarinet," J. Acoust. Soc. Am. **148**, 3827–3835 (2020).
[22]J. W. Thacker and N. Giordano, "Regime change in the recorder: Using Navier-Stokes modeling to design a better instrument," J. Acoust. Soc. Am. **150**, 43–50 (2021).
[23]B. Fabre and A. Hirschberg, "Physical modeling of flue instruments: A review of lumped models," Acta Acust. united Acust. **86**, 599–610 (2000).
[24]H. A. Conklin, Jr., "Piano strings and 'phantom' partials," J. Acoust. Soc. Am. **102**, 659 (1997).
[25]Visualizing the flow in this way is similar, but not exactly the same, as using a vector field showing the flow velocity, as employed in several previous Navier–Stokes—based simulations, for example, in Refs. 26–28.
[26]I. Vaik and G. Paál, "Flow simulations on an organ pipe foot model," J. Acoust. Soc. Am. **133**, 1102–1110 (2013).
[27]T. Kobayashi, T. Akamura, Y. Nagao, T. Iwasaki, K. Nakano, K. Takahashi, and M. Aoyagi, "Interaction between compressible fluid and sound in a flue instrument," Fluid Dyn. Res. **46**, 061411 (2014).
[28]H. Yokoyama, A. Miki, H. Onitsuka, and A. Iida, "Direct numerical simulation of fluid-acoustic interactions in a recorder with tone holes," J. Acoust. Soc. Am. **138**, 858–873 (2015).